MDPI

Article

Sediment Interception by Emergent Stems Across Varying Patch Densities and Flows

Jordan Wingenroth [1*], Candace Yee [2], Justin Nghiem[1,3†] and Laurel Larsen [1,2]

[1] Department of Geography, University of California, Berkeley, CA
[2] Department of Civil and Environmental Engineering, University of California, Berkeley, CA
[3] Department of Statistics, University of California, Berkeley, CA
* Correspondence: j.wingenroth@berkeley.edu
† Current address: California Institute of Technology, Pasadena, CA

Academic Editor: Dr. Rafael Tinoco
Version December 20, 2020 submitted to Geosciences

Abstract: Suspended sediment collected by vegetation in marshes and wetlands contributes to vertical accretion, an important factor in these habitats' futures as sea level rise progresses. Effective capture efficiency (ECE) is a key variable in determining the significance of direct interception in elevation-change models, and one that is not yet thoroughly understood in transitionally turbulent flows. Here we used laboratory flume experiments to determine that ECE decreases with increasing collector Reynolds number (study range: 66 to 200; $p < 0.05$ for 2 of 3 treatments) and collector density (solid volume fraction: 0.22% to 1.17%; $p < 0.05$ for 2 of 3 treatments), and that biofilm has a considerable positive effect on ECE. This is in agreement with previous similar studies. By combining our data with those of the most similar study, we also present a preliminary model quantitatively assessing the effect of collector density on ECE.

Keywords: sediment transport; collector efficiency; submerged vegetation; transitional turbulence; biofilm; sedimentation

1. Introduction

Aquatic flora in many low-elevation marshes and wetlands are at risk of degradation or extirpation due to sea level rise over the course of the 21st century [1,2]. However, vegetation is also hypothesized to play an important role in determining the vertical accretion rate of these same habitats, which factors into their degree of adaptability to sea level rise [3]. In order to better predict sedimentation rates, as well as other properties that are related to sediment transport, such as water quality [4] and ecological productivity [5], quantitative understanding of the ways in which vegetation and suspended sediment interact is required.

Aquatic plants affect sedimentation via numerous mechanisms. Sediment is captured directly on stems, leaves, and other plant surfaces [6,7], and effects of plants on turbulence and flow patterns impact the rate at which suspended particles settle out of the water column due to gravity [8–12]. Furthermore, plants affect bedload transport [13–15] and reentrainment of cohesive [16] and sandy [17] sediment by turbulent flow, which both also impact long-term bed elevation change [16,18]. While gravitational settling plays a dominant role for large or dense particles in typical flow conditions for vegetated reaches [6,9], finer and lighter particles may be destined to either impact vegetation and be captured directly or pass through vegetated areas without being retained.

In our study, we focused specifically on capture efficiency of emergent stems, one of the less well-studied effects of vegetation. Capture efficiency is a geometrical parameter that describes the ability of a collector, usually modeled as a cylinder for vegetation stems, to capture suspended sediment

particles in an open-channel flow (Figure 1). It is calculated as the ratio ($\eta = \frac{w_u}{d_c}$) between the upstream width containing all particles that contact a single collector (w_u) and the collector's diameter (d_c). Effective capture efficiency (ECE; $\eta' = p_r\eta$) accounts for the fact that not all particles coming into infinitesimally close proximity to a collector will adhere to it [19,20], and that affixed particles may later be sheared off [7], thus including probability of retention (p_r) as a multiplicand in its calculation.

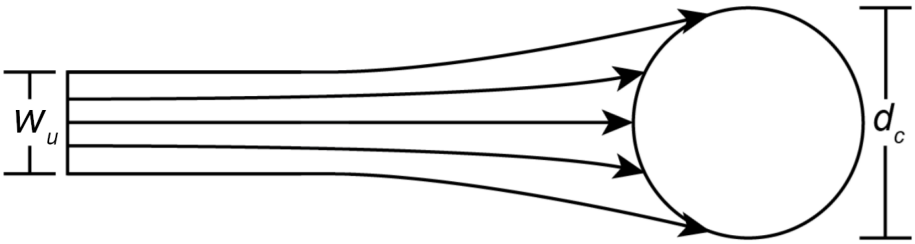

Figure 1. A diagram illustrating capture efficiency for a cylindrical collector. w_u is the horizontal width of upstream flow and d_c is collector diameter. Adapted from Palmer et al. (2004) [21].

Physical properties of collectors, particles, and flow environments are all known to affect capture efficiency, though the relative importance of different mechanisms of effect is still being determined. Greater flow velocities (u) and larger particle diameters (d_p) result in greater direct capture and inertial impaction of particles on stems [21,22]. However, increased u results in increased turbulence—often parameterized by collector Reynolds number ($\mathrm{Re}_c = \frac{ud_c}{\nu}$), where ν is kinematic viscosity—which can trap particles in vortices distant from collector surfaces and shear particles off of collectors, resulting in lower ECE. Increased d_c and spatial density of collectors, which we parameterize as solid volume fraction (ϕ_c), can also result in increased turbulence intensity due to collector wakes, although at sufficiently high densities, decreasing interstitial distance can limit turbulence scale and have a damping effect on turbulent kinetic energy (TKE) [23]. Lastly, biofilm comprising algae, cyanobacteria, and other microorganisms that live on the surfaces of submerged vegetation, has been confirmed to affect capture efficiency [24]. Increased stem roughness [21] seems a likely mechanism, along with possibly improved particle adherence [25].

While analytical expressions have been developed for particle capture in creeping and potential flows [22,26,27], the complexity of the effects described above precludes theoretical solutions for transitional turbulence (approx: $1 < \mathrm{Re}_c < 1000$), which occurs commonly in the environments and on the length scales of aquatic macrovegetation. Hence, empirical estimates are often employed. Palmer [21] introduced a power law expression:

$$\eta = C\mathrm{Re}_c{}^a R^b \,, \tag{1}$$

where C, a, and b are empirically determined regression coefficients. They used an isolated single cylinder coated with grease, for which retention was assumed to be complete ($p_r = 1$), and yielded a model,

$$\eta = 0.224\mathrm{Re}_c{}^{0.718} R^{2.08} \,, \tag{2}$$

with a b coefficient closer to the analytical expression for creeping flows ($O(R^2)$) than that for potential flows ($O(R)$). Wu et al. [28] studied single-collector capture efficiency of colloid particles, which have different physicochemical interactions with collector surfaces, and found a contrasting model:

$$\eta_0 = 0.0044\mathrm{Re}_c{}^{-0.94} N_{\mathrm{Pe}}^{-0.03} \,, \tag{3}$$

where η_0 is contact efficiency, which accounts for $p_r < 1$ due to particles not adhering on initial contact, but still assumes zero resuspension, and N_{Pe} is the Peclet number (ud_c/D, where D is the dispersion

coefficient of the sediment). However, because of their study's focus on laminar flow, their model might not scale to transitionally turbulent conditions.

Before our investigation, two other laboratory studies have examined sediment capture in patches of multiple collectors [24,29]. Purich [29], who also used greased cylindrical collectors, found a negative relationship between η and Re_c for their middle collector-density treatment, but little to no effect—and low absolute η values—for their high- and low-density treatments. Fauria et al. [24] studied artificial leaves as opposed to stems and yielded a new model for ECE in patches of multiple collectors based on the form of Eq. (1):

$$\eta' = C\mathrm{Re}_c{}^{-1.14}R^{0.65}, \tag{4}$$

where C varied depending on their other explicative variables: collector density and biofilm. While they did find higher ECE at lower collector density, and with biofilm present, they only estimated two collector-density treatments, and only determined the effect for biofilm for one of the two. Their study design also did not differentiate enhanced gravitational settling theorized to occur in the proximity of collectors from direct capture on their leaves' surfaces. Perhaps most importantly, neither Fauria et al. nor Purich reported the uncertainty of their respective ECE or η estimates.

With so many variables differing between relatively few studies, additional experimental work is needed to fill in yet unexplored parameter combinations. For example, Eq. (4) has only been tested on leaf-shaped collectors as opposed to vertical cylinders, and the synthetic particulate matter used by Purich [29] has physical properties well outside the range of sediment expected in most natural settings. Our study builds on previous work by testing Eq. (4) for cylindrical collectors across a range of Re_c similar to Fauria et al [24] and an expanded range of multiple ϕ_c values. Additionally, we measure TKE *in situ* to assess its role as a mediator variable between collector density and ECE, delve into the importance of biofilm relative to Re_c and ϕ_c across a range of collector densities, estimate uncertainty in ECE for our particular experimental conditions, and take the first steps towards a quantitative model for ECE as a function of ϕ_c.

2. Materials and Methods

2.1. Experimental Methods

2.1.1. Materials

We conducted our experiments in the Ecogeomorphology flume, an indoor (22.2 +/- 1 °C) recirculating flume located in McCone Hall at the University of California, Berkeley. The flume has a rectangular open-channel section (5.25 m L × 0.6 m W × 0.6 m H) and a bed and sidewalls that are smooth and transparent (Figure 2). At its upstream and downstream ends, this section connects to rectangular ducts with gradually changing hydraulic diameter and rounded corners with curved vertical manifolds along streamlines. These features are intended to maintain laminar flow when water is not affected by collectors. Additionally, at the upstream end of the open-channel, a honeycomb flow collimator served to further straighten flow streamlines before water enters the open channel.

In turn, the ducts guide water to and from the inlet and outlet of the pump array, which consists of a disc pump (Discflo Pumps Corporation, Santee, CA), and a magnetic flowmeter, connected by PVC pipe. This type of pump uses rotating discs to generate viscous drag, which entrains fluid and suspended particles through its interior chamber while maintaining laminar flow and avoiding structural disruption, pulsation, and abrasion [30]. Altogether, the flume design maintains constant, adjustable discharge through the open channel, minimizing background turbulence and other artifacts that arise with other types of pumps.

Within the open channel, we designated a "test section" 1.95 m in length where collectors would be installed. This test section and the surrounding area were instrumented with the following devices:

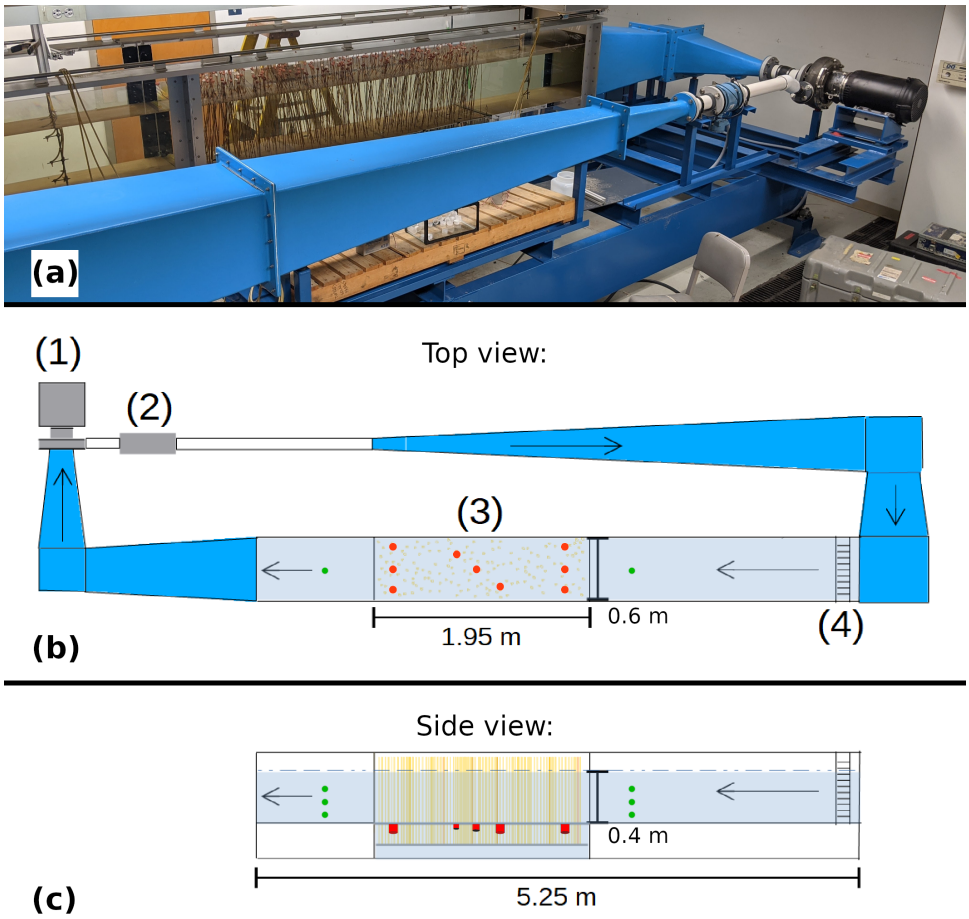

Figure 2. The Ecogeomorphology flume. Not all measurements are to scale. **(a)** Photograph of the test section (center-left) and pump (right). **(b)** Conceptual diagram of the flume as seen from above. Labeled parts are: 1) pump, 2) magnetic flowmeter, 3) test section, and 4) honeycomb flow collimator. Arrows indicate direction of flow. Green points represent the inlets for the peristaltic pumps sampling suspended particle concentration. Red areas represent the sediment traps. **(c)** A side view of the open-channel part of the system.

1. A flat-bedded array positioned flush with the neighboring channel bed, containing vertical, emergent collector stems, which were spaced uniformly in an unpatterned manner
2. Two battery-operated peristaltic pumps (Cole-Parmer, Vernon Hills, IL) used to sample suspended particle concentration via three hose inlets each (inside diameter = 3.1 mm), which were suspended at a range of heights from the channel bed (5; 14; 27 cm); these were positioned 50 cm upstream and downstream of the test section
3. sediment traps (n = 9) with 2.5 cm circular openings flush with the bed and collection filters (Whatman GF/F) on perforated filter holders recessed in a 5 cm deep cylindrical cavity (trap Reynolds number and aspect ratio chosen to minimize bias [31]); these were interspersed among the collectors in a grid-like pattern

We used 1/8" (0.3175 cm) cylindrical wooden dowels as collectors, which were covered in silicone grease (Chemplex 710, Fuchs Petrolub, Mannheim, Germany) in order to retain impacted particles and spread randomly throughout the test section at the appropriate density. Crushed walnut shell was used as a substitute for suspended sediment because it has surficial and physical properties comparable to the organic-rich types common in wetlands [32–34]. We used WF5-200 grade (Composition Materials Co., Milford, CT), which passes entirely through a #60 sieve (250 µm), and which we determined has a average particle diameter (d_{50}) of 25.2 µm based on measurements using a

laser-scattering-based instrument (LISST-Portable | XR, Sequoia Scientific, Bellevue, WA; See Appendix A1). We also empirically estimated the particle density for this specific walnut shell flour to be 1.53 g/cm^3 using volume displacement.

2.1.2. Suspended Particle Concentration Analysis

We conducted experimental runs for a fully-crossed parameter space of collector Reynolds number (67; 134; 200) and collector density (0; 285; 821; 1487 collectors/m^2 bed area). These values, as well as other experimental parameters held constant throughout, were chosen because they correspond to those that might occur for emergent grasses or reeds in natural settings (Table 1). A zero-collector control density was included in order to isolate the effects of our experimental installations from the background effects of the rest of the flume.

Table 1. Experimental and natural parameter ranges. Natural values are based on approximations or measurements from cited studies and literature reviews in wetlands or other low-elevation flows.

Parameter	This study	Fauria et al. (2015)	Purich (2006)	Natural
Flow velocity (cm/s)	2.0–6.0	1.8–6.1	1.0–10.2	0–25 [35]
Flow depth (cm)	40	14–17	12	0–50 [36]
Collector shape	Cylindrical	Artificial grass	Cylindrical	Varies
Collector diameter (cm)	0.318	0.3	0.6	0.1–1.2 [37,38]
Collector Reynolds number	66–200	54–183	70–640	5–1000 [36]
Collector density (#/m^2)	285–1487	2724–7209	1013–4053	10–2700 [38]
Solid volume fraction (%)	0.22–1.17	0.82–2.16	2.86–11.5	0.1–1 [37]
Particle type	Walnut shell	Road dust	Pliolite®	Sediment
Particle density (g/cm^3)	1.53	2.27–2.61 [1]	1.03	1.43–2.39 [34]
Average particle diameter, d_{50} (µm)	25.2	∼10–15 [2]	212–250	45–100 [39,40]
Suspended concentration (µL/L)	5–55	<9–50 [2]	∼110	2-25 [40,41]
Particle-collector diameter ratio, R	0.0079	0.0004–0.083 [2]	0.037	<0.25

[1] Estimated from a different study about road dust properties [42]
[2] Fauria et al. [24] used a LISST to measure capture in separate bins across a broad range of particle diameters (1.25–250 µm) rather than overall suspended concentration

Before each experiment, the flume was filled with tap water to 0.4 m depth in the test section, which was enough to fully submerge the pump and almost the entirety of the duct length. At this depth, the volume of water in the entire flume was approximately 2.43 m^3 (See Appendix A2). A Nortek Vectrino Profiler ADV (acoustic Doppler velocimeter; Nortek AS, Vangkroken 2, 1351 Rud, Norway) was used to calibrate the pump to generate channel mean flow velocities (2.0; 4.0; 6.0 cm/s) within the pump's capabilities and corresponding to the range of interest for Re_c. At these flow rates (0.0048; 0.0096; 0.0144 m^3/s), circulation times for the entire system were 506 s, 253 s, and 169 s, respectively. The drag caused by collectors was not found to detectably affect upstream or downstream flow velocities.

Sediment traps were installed immediately before each run, then a slurry consisting of 200 g of crushed walnut shell suspended in 15.1 L of tap water was added using a spigot calibrated to finish draining after a period roughly equal to circulation time (3 minutes). Test-section flow velocity was kept at 6 cm/s for this period across Re_c treatments, then adjusted to the appropriate value for the treatment. This procedure was intended to make particle concentration longitudinally even throughout the system. Estimated depth-averaged starting concentration was 82.3 mg/L (53.8 µL/L).

In preliminary experiments, we determined 100 minutes was more than adequate to capture the effects of settling and capture on suspended concentrations across our parameter space. We sampled suspended concentration using the peristaltic pumps every 5 minutes, the first sample occurring 5 minutes after we began adding sediment to the flume. Samples measured approximately 140 ml each, and our sampling frequency resulted in 19 sampled timesteps per experiment, with six samples

per timestep. sediment traps were covered with a plunger and removed at 100 minutes, so the last peristaltic pump sample occurred at 95 minutes due to personnel limitations.

Peristaltic pump samples were processed using vacuum filtration. Before filtration, quantitative glass microfiber filter papers (Whatman GF/F) were oven-dried for 24 hours at 40 °C to remove any moisture, weighed, and assigned to a flume sample. The volume of flume water passed through the filter was measured, then the drying and weighing process was repeated to estimate the mass of sediment on the filter. Concentrations were recorded in mg/L. Filter papers from sediment traps were dried and weighed before and after the run in a similar fashion, to estimate the mass of settled particles they contained.

2.1.3. Estimating Collector-Induced Turbulence

We estimated mid-water-column turbulent kinetic energy (TKE) among the collectors for each combination of Re_c and collector density using the Vectrino Profiler ADV. The Vectrino was mounted on a frame suspended above the test section and adjusted until its bottom-depth measurement read 15 cm. A bubble level was used to ensure it was oriented along the vertical axis. The ADV measured velocity in two horizontal dimensions, and two separate measurements along the vertical dimension, at a frequency of 10 Hz. It also collected other data such as autocorrelation and signal-to-noise ratio. We collected 5 minutes of data per treatment in the interest of including the vast majority of expected periodicity in our variance measurement. Measurements taken by the ADV were filtered, leaving out timepoints where the two vertical velocity measurements differed by 50% or more or the SNR measurement was greater than 5 dB, and were subsequently despiked using a phase-space thresholding algorithm [43]. TKE was derived from the cleaned Vectrino data as half the sum of the variances of the velocity components:

$$\mathrm{TKE} = \frac{1}{2}[\overline{(u')^2} + \overline{(v')^2} + \overline{(w')^2}]\,. \tag{5}$$

2.1.4. Biofilm Growth

The effect of biofilm on the surficial properties of collectors, and thereby their effective capture efficiency, was another factor of interest for our experiment. While we did not incorporate biofilm into the fully-crossed parameter space of other explicative variables due to the time-intensiveness of growing algae, we did carry out an auxiliary experiment to roughly assess its effect size. After one of the experiments at each collector density, the water in the flume was allowed to come to rest, then the collectors sat constantly illuminated by one white, fluorescent grow-light for a measured number of days. The crushed walnut shell doubled as a food source for the microorganisms constituting the biofilm, which we observed grew plentifully in all cases.

Once biofilm became visually apparent on the collectors' surfaces, an experiment was conducted using the same materials and protocols as the treatments without biofilm, holding $\mathrm{Re}_c = 200$ constant between biofilm treatments. The length of time it took for robust biofilm growth to occur differed between the low, medium, and high collector-density treatments (13; 18; 20 days, respectively). For the highest collector-density treatment, a follow-up experiment with a longer growth period (46 days) was performed. While we did not quantitatively assess biofilm mass, we assumed that the number of days it was allowed to grow could be used as a proxy, acknowledging that the growth rate (in mass units per day) was probably exponential or logistic rather than linear.

2.2. Sediment Transport and Particle Capture Model

2.2.1. Model Derivation

We used an exponential decay model for suspended sediment concentration adapted from Fauria et al. [24] to estimate ECE (η'):

$$\frac{\mathrm{d}\bar{\phi}}{\mathrm{d}t} = -\left[\frac{C_b v_s}{h}(1-E_r) + \eta' u d_c I_c\right]\bar{\phi}(t) = -(k_s + k_c)\bar{\phi}(t) = -k\bar{\phi}(t)\,. \tag{6}$$

$\bar{\phi}(t) = \frac{1}{h}\int_0^h \phi(z)\,\mathrm{d}z$ is the depth-averaged suspended sediment concentration at time t, where h is water depth, z is height above the bed, and $\phi(z)$ is concentration at height z. $k_s = \frac{C_b v_s}{h}(1-E_r)$ is the exponential time-decay rate of $\bar{\phi}$ due to settling, which is calculated from settling velocity (v_s), h, a constant (C_b) that accounts for the concentration near the bed predicted by the Rouse equation relative to $\bar{\phi}$, and a dimensionless rate at which particles are entrained from the bed (E_r). Further derivation of k_s is available in Fauria et al. [24]. $k_c = \eta' u d_c I_c$ is the rate at which particles are removed from suspension due to capture by collectors. $I_c = \frac{N_c h}{V}$ is collector height density, where N_c is the total number of stems, and V is the volume of water in which stems are contained.

The solution of the differential equation (Eq. (6)) is exponential,

$$\bar{\phi}(t) = \bar{\phi}(0)e^{-kt} = \bar{\phi}(0)e^{-(k_s+k_c)t}\,. \tag{7}$$

Concentration at any height can be assumed to change over time in proportion to average concentration because we assume the vertical profile of sediment concentration maintains a constant shape governed by the Rouse equation [44],

$$\frac{\phi_z}{\phi_r} = \left(\frac{h-z}{z}\frac{z_r}{h-z_r}\right)^{R_0}\,, \tag{8}$$

where ϕ_r is concentration at an arbitrary reference height above the bed (z_r), conventionally $0.05h$, and R_0 is referred to as the Rouse number [45].

To calculate k_s, we began by calculating the average mass of sediment that settled per sediment trap over the duration of the experiment (100 minutes). We then scaled this measurement up from the area of a sediment trap's horizontal opening (5.07×10^{-4} m^2) to the total test section bed area (1.17 m^2). The resulting estimate of the sediment mass settled in the test section (m_s) was divided by the total mass removed from suspension during a run to calculate the proportion of the decrease due to settling. This proportion was multiplied by the total exponential decay coefficient, k, to calculate k_s:

$$k_s = \frac{m_s}{m_0(1-e^{-kT})}k\,, \tag{9}$$

where m_0 was the mass of sediment suspended at the beginning of the experiment and T was the total duration of the experiment.

The equations above model the dynamics occurring in the test section alone. To account for settling and reentrainment outside the test section, a background exponential decay rate (k_b) was estimated from runs with zero collectors for each Re_c treatment ($k_c = 0 \implies k_b = k - k_s$). ECE for our collector-density treatments was then calculated from k_c. Also, because collectors only act on suspended particles while they are passing through the test section, this estimate for ECE was scaled by the ratio (5.19) between the total volume of water in the flume (2.43 m^3) and $V = 0.468$ m^3:

$$\eta' = 5.19\frac{k_c}{u d_c I_c} = 5.19\frac{k - k_s - k_b}{u d_c I_c}\,. \tag{10}$$

2.2.2. Model Execution

In order to correct for observed heteroscedasticity (See Appendix A3) across time, with earlier, higher-concentration measurements showing greater variance, we log-transformed the exponential model (Eq. (7)). This resulted in a linear model taking the form,

$$log(\bar{\boldsymbol{\phi}}) = log(\bar{\phi}(0)) - k\boldsymbol{t} + \boldsymbol{U}\,, \tag{11}$$

which was evaluated for each experimental configuration separately. Bold font signifies vector variables, and $\boldsymbol{U}$ is the random error term of the model. The standard error of this k term and the standard deviation of m_s estimates from sediment traps were propagated through Eqs. (9) and (10), for both control and treatment runs, and were ultimately used to calculate uncertainty estimates for ECE.

Our experiment collected suspended concentration samples at three different heights and both upstream and downstream of the test section. Because the observed magnitude of the Rouse profile (Eq. (8)) and the upstream-downstream difference were barely detectable with our degree of precision, and both were negligible relative to the concentration decay over time, we opted to pool data from all six suspended sediment sampling locations rather than complicating the model further. While we might overestimate or underestimate absolute concentration this way, exponential decay is expected to be constant across height on account of the constant Rouse profile, and thus estimated ECE would not be affected.

We used a Monte Carlo approach to assess the significance of the effects of Re_c and ϕ_c on ECE. For each combination of Re_c and ϕ_c, 30,000 random values were drawn from a normal distribution whose mean equals that combination's empirically estimated ECE and whose standard deviation equals its standard error (SE). These values were log-transformed, since we expected the relationships to fit a power-law model. For each stratum of a given explicative variable, sets (triplets) with one randomly sampled value from each of the strata of the other explicative variable were regressed using ordinary least squares, producing a roughly normal distribution of coefficients (n = 30,000) for each level of both variables (6 total). The distributions of slopes were used in two-tailed t-tests (null hypothesis: $\mu = 0$; $\alpha = 0.05$) to determine the significance of relationships.

Lastly, we compared our results to Fauria et al. [24] by fitting their model (Eq. (4)) to our data at each of our collector densities, estimating C, then fitting a power-law function relating the combined C values from their study and ours to collector density. C is directly proportional to ECE in their model, so this can be thought of as an indirect way to quantify the relationship between collector density and ECE.

3. Results

3.1. Particle Capture

Effective capture efficiency was found to decrease with increasing Re_c and ϕ_c throughout our parameter space, with one exception. This exception occurred at the lowest collector density ($\phi_c = 0.22\%$), where the intermediate Re_c treatment ($\mathrm{Re}_c = 134$) had lower ECE than both the lower and higher Re_c treatments (Figure 3a). When compared to the other collector-density treatments with the same Re_c value, this low collector-density experiment's calculated ECE was slightly lower than the intermediate collector-density treatment, and was greater than the highest collector-density treatment (Figure 3b). Our experimental uncertainty was great enough that this might be attributable to random error. However, repeating the experiment with the same parameters yielded a nearly identical result (omitted from analysis).

Monte Carlo analysis determined that there is a significant negative relationship between ECE and collector density for the low (p = 0.004) and high (p = 0.019) Re_c treatments, but no significant effect was detected (p > 0.05) for the intermediate treatment (Figure 4a). We also found a significant negative relationship between ECE and Re_c for the low (p = 0.026) and high (p = 0.046) collector-density treatments, but an insignificant (p > 0.05) trend for the intermediate collector-density treatment (Figure 4b).

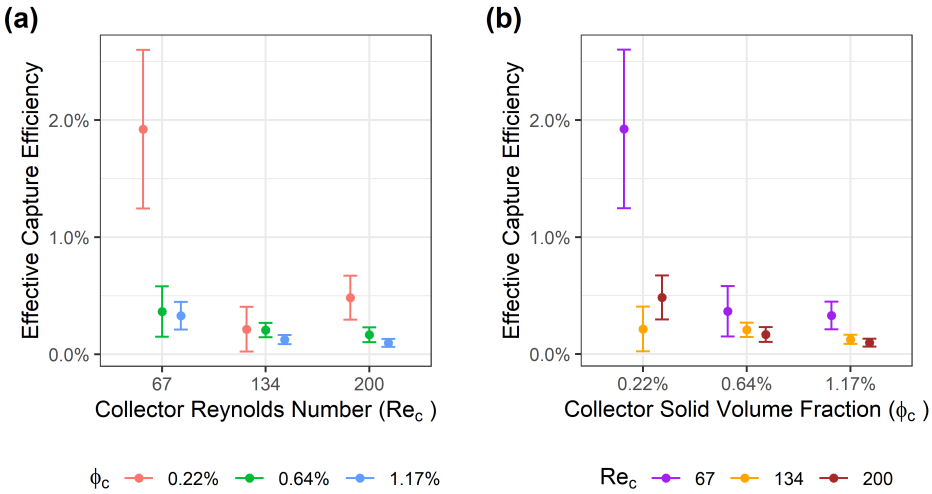

Figure 3. Estimates of effective capture efficiency calculated from laboratory experiments across the collector density × Reynolds number (Re_c) parameter space. Error bars represent +/- 1 SE. (**a**) Estimates plotted over Re_c, colored by solid volume fraction (ϕ_c). (**b**) Estimates plotted over ϕ_c, colored by Re_c.

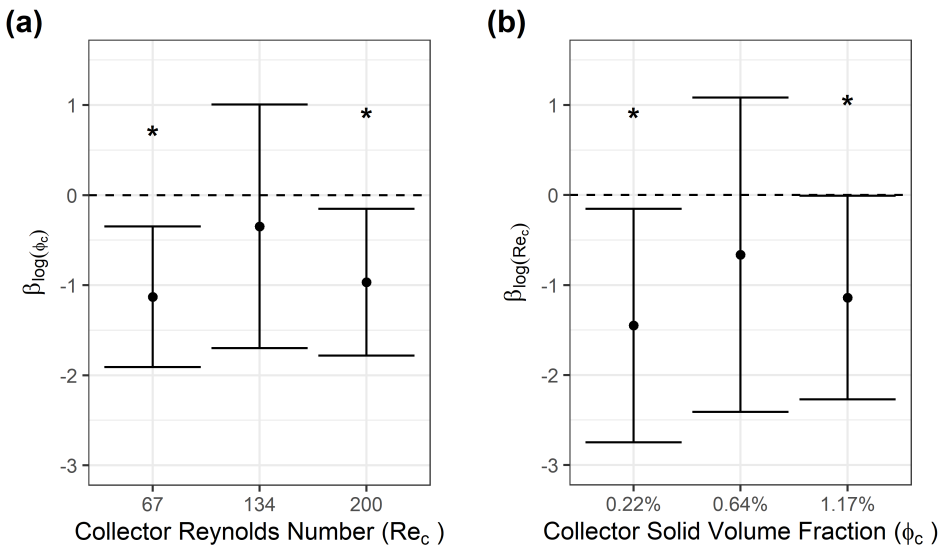

Figure 4. Effect size estimates from Monte Carlo regression analysis. Error bars represent 95% confidence intervals. Asterisks mark the parameter values at which the effect size was found to be significant. (**a**) Estimates of the effect of log-transformed collector solid volume fraction ($\beta_{\log(\phi_c)}$) on ECE, stratified by Re_c. (**b**) Estimates of the effect of log-transformed Re_c ($\beta_{\log(\mathrm{Re}_c)}$) on ECE, stratified by solid volume fraction (ϕ_c).

3.2. Turbulence

TKE was consistently found to increase with increasing flow velocity as expected (Table 2). Generally, higher collector density also led to greater turbulence, with the greatest increase in terms of both absolute and relative magnitude taking place between the lower and middle collector-density treatments. A slight decrease actually occurred thereafter (between the middle and highest collector densities) for the middle and highest Re_c treatments, with a slight increase for the lowest Re_c treatment. The similarity of TKE for the upper two collector-density treatments suggests a potential

threshold occurring before or near the middle treatment's ϕ_c value. ECE and TKE exhibited a negative relationship across the experimental parameter space (n = 9) taken as a whole (Figure 5).

Table 2. Turbulent kinetic energy (TKE) for all collector solid volume fraction (ϕ_c) and Re_c treatments, including the control (zero-collector) treatments for reference.

ϕ_c	Re_c	**mid-water-column TKE** ($\mathrm{mm}^2/\mathrm{s}^2$)
Control	**67**	2.48
	134	2.98
	200	3.37
0.22%	**67**	1.23
	134	5.26
	200	12.2
0.64%	**67**	9.13
	134	35.9
	200	59.6
1.17%	**67**	11.1
	134	29.8
	200	54.4

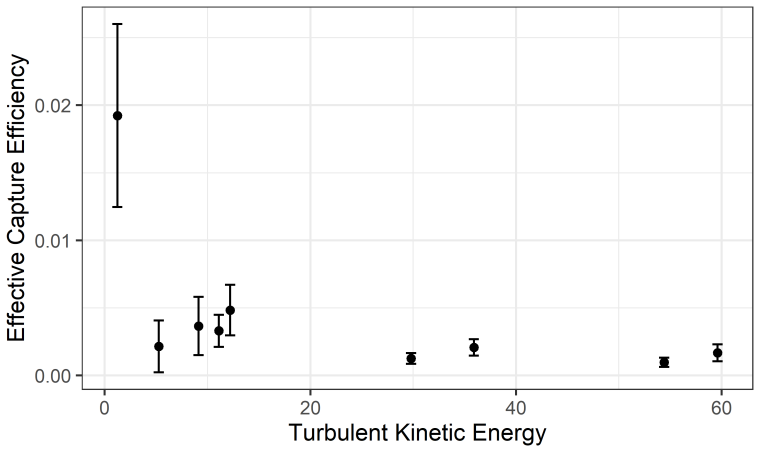

Figure 5. Effective capture efficiency as a function of turbulent kinetic energy for all experimental treatments studied.

3.3. Biofilm Effects

We observed robust biofilm growth, consistent throughout the test section. Biofilm grew on the surfaces of collectors and, as we discovered after turning the pump on, in strands (less than 5 cm long) that were pulled downstream by the flow. Biofilm growth was consistently found to increase ECE (Figure 6). For the runs conducted when biofilm was first observed to be abundant in the test section (13-20 days), both absolute (+0.71% ECE) and relative (an improvement to 2.48 times control) increase were greatest by a considerable margin at the lowest collector density, which also had the shortest growth period (13 days). The middle and highest collector densities were fairly close in terms of absolute increase (+0.09% ECE and +0.07% ECE, respectively) and relative increase (1.53 times and 1.73 times, respectively). Interestingly, in our test of a longer grow time (46 days) at the highest collector density, ECE increased with far greater relative (7.15 times) and absolute (+0.60% ECE) magnitude, suggesting that the other runs might not have been at saturation in terms of biofilm mass.

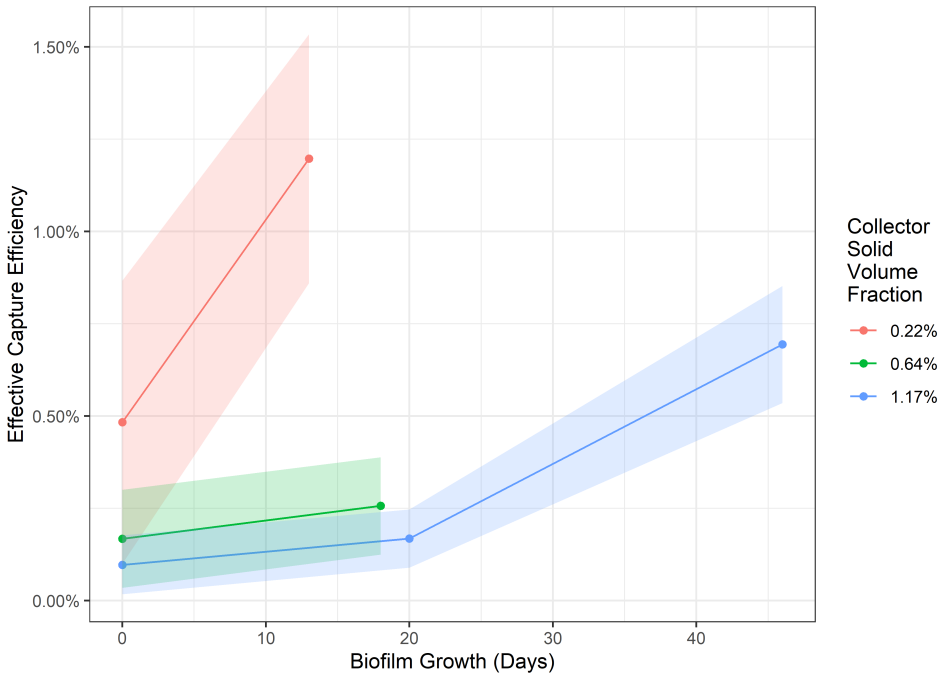

Figure 6. Estimates of effective capture efficiency calculated from experimental runs with varying degrees of biofilm growth. Colors represent the different collector densities, expressed as solid volume fraction (ϕ_c). Straight lines are drawn between the points that represent our experiments and the shaded areas represent 95% confidence intervals for ECE inferred from our measurement uncertainty.

3.4. Comparison to Previous Models of Capture Efficiency

Aside from the outlier at the mid Re_c, lowest collector-density treatment, all of our observations were in agreement with the power-law model from Fauria et al. [24] (Figure 7). In no other case did the model prediction differ from our empirical observation by more than 1 standard error (SE). Moreover, the model relating C to ϕ_c yielded marginally good fit (R^2 = 0.82):

$$C = 0.00801{\phi_c}^{-1.41}\,. \tag{12}$$

It underestimated C for all of our collector-density treatments, and overestimated it for both of those from Fauria et al. (ϕ_c = 0.82%, 2.16%). However the magnitude of this error was small in comparison to the absolute differences in C among the various ϕ_c values (n = 5). Data scarcity should be considered a limiting factor in the interpretation of these results.

4. Discussion

4.1. Inferred Mechanisms of Effect for Collector Density and Reynolds Number

It is notable that the exponential coefficient for ϕ_c as a predictor of C (Eq. (12)), and thus indirectly ECE, is greater in magnitude than those found by Fauria et al. [24] for either Re_c or R as a direct predictor of ECE. With the evidence of a positive—albeit potentially thresholded—effect of collector density on TKE, and the evidence of TKE's negative effect on ECE, it seems likely that secondary turbulence generated by upstream collectors negatively affects downstream collectors' ECE. This is conceptually valid because greater fluctuations in flow velocity exert stronger forces with more variable directionality on sediment particles affixed to collectors, increasing the probability of resuspension.

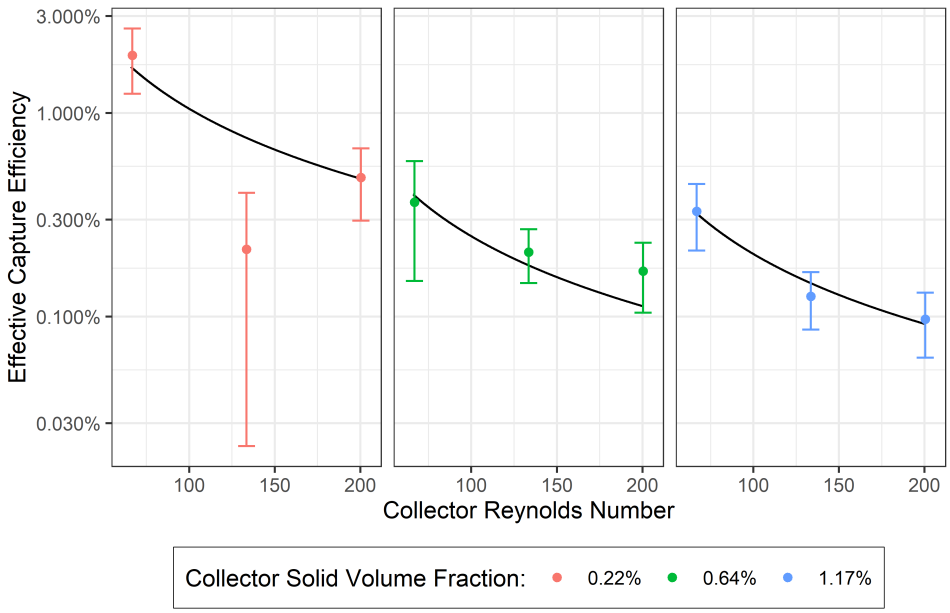

Figure 7. A comparison of our experimental estimates of effective capture efficiency, colored according to collector solid volume fraction (ϕ_c), and the predictions of the Fauria et al. [24] power law model (black lines). Effective capture efficiency is plotted on a log scale in order to display model fit more precisely at small values. Error bars represent +/- 1 SE.

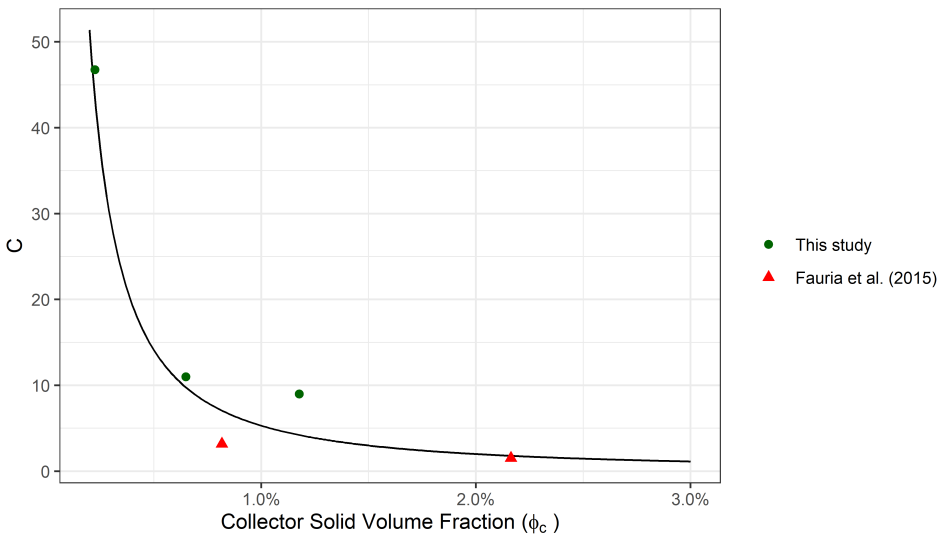

Figure 8. A comparison of the *C* values calculuated for each of our collector-density treatments to those calculated by Fauria et al. [24]. The black line represents the power-law model of best fit between *C* and collector solid volume fraction (ϕ_c) for our collector-density treaments and those of Fauria et al. combined (n = 5), for which R^2 = 0.82.

The threshold in TKE's relationship with collector density likely indicates that the turbulent eddy scale and the distance between collectors converged somewhere in our parameter space, so that additional collectors acted to damp eddies as much or more than they acted to create them. Accounting for secondary turbulence in future models and experiments seems feasible and important. In general, moving on from the simplistic power-law models developed initially as a way to bridge the gap between analytical expressions for creeping and potential flows to more theoretically-grounded empirical models [46] seems a promising avenue for future investigation.

The ECE of 1.92% that we observed at our lowest Re_c and collector-density treatment is one of the highest observed in any laboratory experiment with multiple collectors [46]. Our observation did fall above the value (1.67%) predicted by the Fauria et al. model [24] that was fit at that collector density. However, the anomalous experiment at the middle Re_c treatment that also influenced that model's fit (Figure 7) probably explains some or all of that difference. Repeating the experiment with the same parameters failed to rectify the anomaly, since it yielded a similar ECE estimate.

On the whole, our results demonstrate that the Fauria et al. model remains a reasonably good predictor of ECE even at collector densities lower than those they studied, and add to the pool of evidence that ECE in settings with multiple stems has a negative relationship with Re_c [24,25], as opposed to the positive relationship between η and Re_c observed for sediment in settings with only one stem [21].

We attribute that difference in part to resuspension driven by turbulent wakes from upstream stems. It is noteworthy that we observed a negative effect despite greasing our stems with the same product and protocol used by Palmer [21], calling into question previous assumptions that $p_r = 1$ for greased dowels. While Purich [29] did empirically confirm resuspension from their greased collectors was low, they did so based on a dowel holding relatively few particles (n = 35). If those particles were added manually before the test, or if they remained on the dowel throughout agitation when others might have been removed, they might not reflect the average resuspension behavior of captured particles.

4.2. Relative Importance of Biofilm

The presence of biofilm, which is thought to predominantly affect particle adherence and retention, was found to have a substantial positive effect on ECE. Because Fauria et al. [24] already confirmed that the negative effect of Re_c on ECE is supported both with and without biofilm present, and because the duration of growth makes biofilm runs quite time-intensive, we focused solely on collector density's interactions with biofilm. Roughly equivalent biofilm growth (visibly apparent after 13-20 days) resulted in similar relative increase of ECE across our collector density parameter range (improvement to 1.53–2.38 times control), despite quite different absolute values of ECE. As Fauria et al. [24] found for Re_c, biofilm-positive runs—like biofilm-negative runs—exhibited consistent decline in ECE with increasing collector density.

Absolute effects of biofilm were on par with those of Re_c and collector density across our parameter space. At the Reynolds number (200) used for biofilm experiments, ECE ranged from 0.10% to 0.48% across our collector-density treatments without biofilm, for an effect size of 0.38%, and absolute effects of biofilm ranged from +0.07% ECE to +0.71% ECE. Absolute effects of Re_c (0.20%–1.71% ECE) on ECE for specific collector densities were larger than the biofilm effect sizes by a ratio of roughly 2.5:1. This demonstrates biofilm's effect is on the same order of magnitude as the other variables, but the fact that our parameter ranges span a subset of reasonable natural values means that these comparisons should be considered to be inexact.

The multiplicative nature of biofilm's relationship with ECE, and biofilm's apparent importance relative to other factors, makes incorporating quantitative measures of biofilm in future models for ECE seem like a promising avenue. We are unable to do so here because we did not measure biofilm growth quantitatively, aside from our effort to standardize it across treatments of the other variables. To develop such a model, more sophisticated hydroponic equipment to monitor and account for factors impacting growth rate [47,48], and protocols for measuring the mass and other characteristics of biofilm grown [49,50], should be incorporated in future experiments. Additionally, the strands we observed forming on collectors led us to question the relative proportion of capture due to filamentous versus surficial biofilm, another question in need of investigation.

4.3. Designing Wetlands for Maximum Sedimentation

Supplementary Materials: The following are available online at http://www.mdpi.com/2076-3263/TBDXX/TBDYY/TBDZZ/s1, Figure S1: title, Table S1: title, Video S1: title.

Author Contributions: Conceptualization, L.L., J.N., and J.W.; methodology, L.L. and J.W.; software, L.L., J.N., J.W., and C.Y.; validation, J.W.; formal analysis, J.W. and C.Y.; investigation, J.N., J.W, and C.Y.; resources, L.L.; data curation, J.W.; writing–original draft preparation, J.N., J.W., and C.Y.; writing–review and editing, L.L., J.N., J.W., and C.Y.; visualization, J.W.; supervision, L.L., J.W., and C.Y.; project administration, L.L. and J.W.; funding acquisition, L.L.

Funding: This research was funded by NSF award #1455362.

Acknowledgments: The authors wish to thank and acknowledge Colin Keating and Aaron Hurst for their helpful work on preliminary flume experiments. We also wish to express great thanks to Yayla Sezinger, Elle Chen, Nicole Ulakovic, Katrina Ginsberg, and Danielle Satin for their time spent preparing for experiments, maintaining the flume, and fastidiously carrying out other important laboratory tasks. Lastly, we wish to thank Sam Stein and Sheila Trampush for graciously sharing data and participating in brainstorming sessions while working on concurrent studies within the same general topic area.

Conflicts of Interest: The authors declare no conflict of interest.

Abbreviations

The following notations are used in this manuscript:

η	particle capture efficiency, dimensionless
w_u	upstream width of streamlines that intersect a collector, cm
d_c	collector diameter, cm
η'	effective capture efficiency (ECE), dimensionless
p_r	probability of particle retention, dimensionless
d_p	particle diameter, µm
Re_c	collector Reynolds number, dimensionless
u	flow velocity, cm/s
ν	kinematic viscosity cm^2/s
R	particle-collector diameter ratio, dimensionless
C, a, b	power-law coefficients (Eq. (1)), dimensionless
$\bar{\phi}$	depth-averaged suspended sediment concentration, µL/L
t	time, s
h	water depth, cm
z	height above the bed, cm
ϕ_z	suspended sediment concentration at height z, µL/L
k_s	concentration time-decay due to settling, s^{-1}
v_s	settling velocity, cm/s
C_b	constant relating near-bed concentration to depth-averaged concentration, dimensionless
E_r	entrainment rate, dimensionless
k_c	concentration time-decay due to capture, s^{-1}
I_c	collector height density, m/m^3
N_c	number of collectors, #
V	test section water volume, m^3
z_r	reference height (Eq. (8)), cm
ϕ_r	suspended sediment concentration at reference height z_r, µL/L
R_0	Rouse number, dimensionless
m_s	sediment mass settled in test section, g
m_0	sediment mass suspended at beginning of experiment, g
T	total duration of experiment, s
k_b	background concentration time-decay, s^{-1}
ϕ_c	collector solid volume fraction, dimensionless

Appendix A. Secondary methodology

Appendix A.1. Particle Size

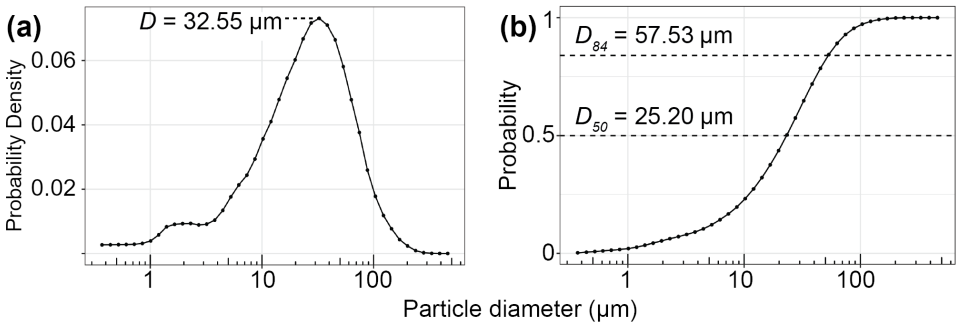

Figure A1. Walnut shell flour (WF5-200) particle size distribution, as measured by LISST-XR | Portable. (**a**) Probability density function, with mode (32.55 µm) indicated. (**b**) Cumulative density function, with 50th (25.20 µm) and 84th (57.53 µm) percentiles highlighted.

Appendix A.2. Flume Volume

In order to estimate ECE, we need to know the particle capture rate for water that is being acted upon by the collectors (i.e., in the test section). This requires scaling up by the ratio between the test section volume (1.95 m $\times$ 0.6 m $\times$ 0.4 m = 0.468 m^3) and the water volume of the flume's entire wetted floorplan under experimental conditions (depth = 0.4 m in test section). Because of the flume's irregular floorplan and shape, estimating its water volume theoretically is impractical, and technical documents were calculated at a different water depth, so we made an empirical estimate.

We drained the flume after an experiment while measuring flow rate at the drain outlet over time, performed polynomial regression (Figure A2), and calculated a definite integral ($V = \int_{t_{full}}^{t_{empty}} -\frac{dV}{dt} dt$) from when draining began to when the part of the flume involved in the experimental flows was empty . Because polynomials of second order and above fit well and yielded very similar volume estimates, we felt confident using 2.43 m^3 as the flume volume in our calculations (Table A1).

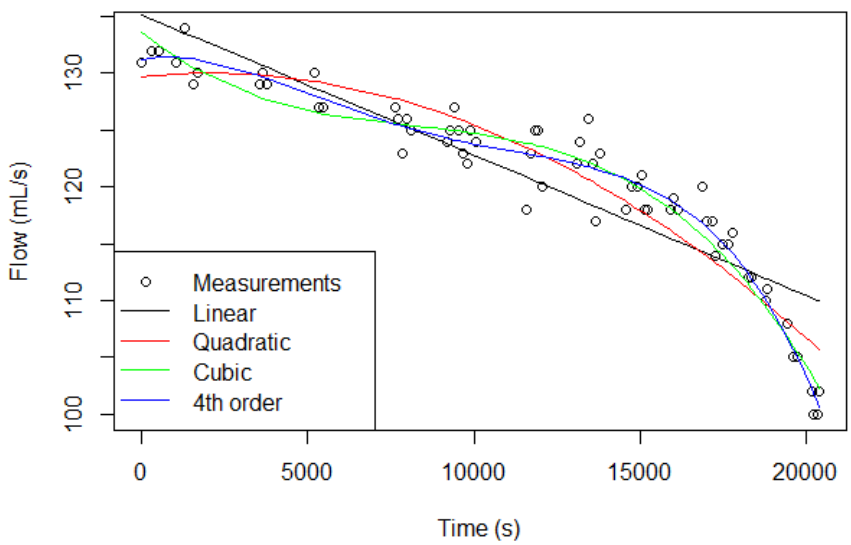

Figure A2. Polynomial models predicting the rate at which the flume drained, to be integrated to estimate the volume in circulation during experiments.

Table A1. Polynomial model summary

Model	Estimated Volume (m^3)	R^2
Linear	2.4309	0.80
Quadratic	2.4277	0.90
Cubic	2.4373	0.94
4th-order	2.4294	0.96

Appendix A.3. Heteroskedasticity Reduction

Because measurement error was proportional to sample concentration, which was greater at the beginning of experiments than at the end, heteroskedasticity was observed in our suspended concentration data. We log-transformed the data and then performed linear regression, confirming that heteroskedasticity was reduced in comparison to least-squares exponential regression on the raw data (Figure A3). While it would be preferable to also address non-randomness (i.e., curvature) in the residuals *post hoc*, subsetting data across time is not advisable because k_s was calculated for T, the total run duration.

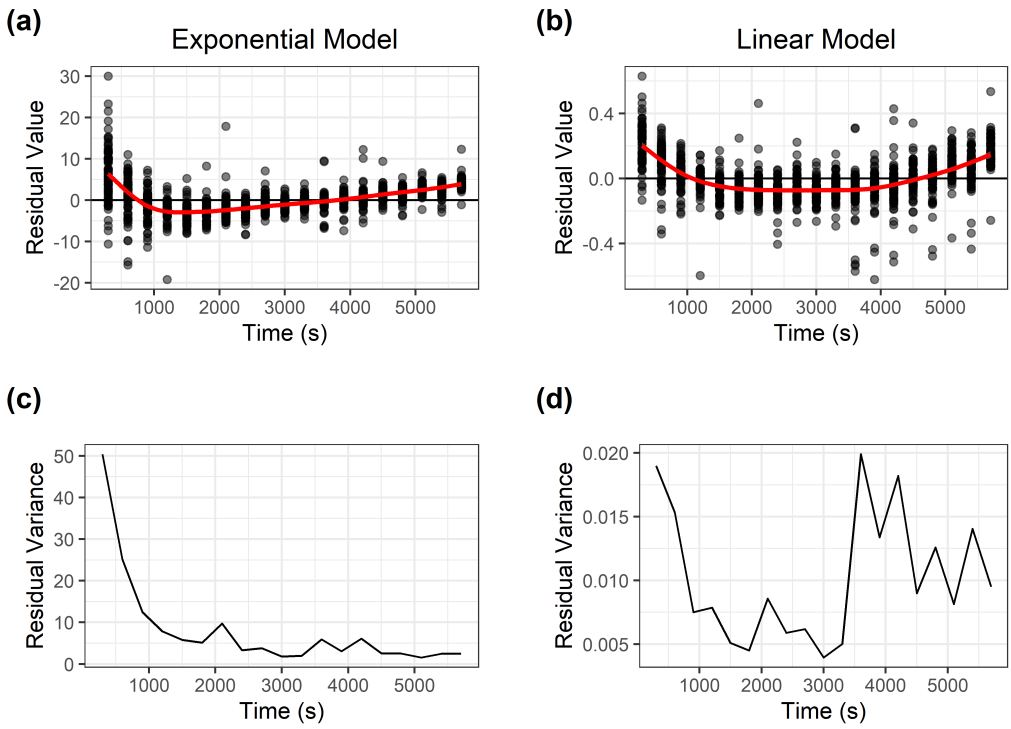

Figure A3. Plots of residuals and residual variance pooled from all 12 experimental treatments including controls. Red lines are locally-weighted smoothing functions **(a)** Residuals of the exponential model. **(b)** Residuals of the transformed linear model used in analyses. **(c)** Variance of the residual values of the exponential model. **(d)** Variance of the residual values of the linear model used in analyses.

References

1. Thorne, K.; MacDonald, G.; Guntenspergen, G.; Ambrose, R.; Buffington, K.; Dugger, B.; Freeman, C.; Janousek, C.; Brown, L.; Rosencranz, J.; others. US Pacific coastal wetland resilience and vulnerability to sea-level rise. *Science Advances* **2018**, *4*, eaao3270.
2. Jankowski, K.L.; Törnqvist, T.E.; Fernandes, A.M. Vulnerability of Louisiana's coastal wetlands to present-day rates of relative sea-level rise. *Nature Communications* **2017**, *8*, 1–7.

3. Kirwan, M.L.; Guntenspergen, G.R.; D'Alpaos, A.; Morris, J.T.; Mudd, S.M.; Temmerman, S. Limits on the adaptability of coastal marshes to rising sea level. *Geophysical research letters* **2010**, *37*.
4. Goodwin, T.H.; Young, A.R.; Holmes, M.G.; Old, G.H.; Hewitt, N.; Leeks, G.J.; Packman, J.C.; Smith, B.P. The temporal and spatial variability of sediment transport and yields within the Bradford Beck catchment, West Yorkshire. *Science of the Total Environment* **2003**, *314*, 475–494.
5. Kirwan, M.L.; Murray, A.B. A coupled geomorphic and ecological model of tidal marsh evolution. *Proceedings of the National Academy of Sciences* **2007**, *104*, 6118–6122.
6. Mudd, S.M.; D'Alpaos, A.; Morris, J.T. How does vegetation affect sedimentation on tidal marshes? Investigating particle capture and hydrodynamic controls on biologically mediated sedimentation. *Journal of Geophysical Research: Earth Surface* **2010**, *115*.
7. Peruzzo, P.; Defina, A.; Nepf, H. Capillary trapping of buoyant particles within regions of emergent vegetation. *Water Resources Research* **2012**, *48*.
8. Christiansen, T.; Wiberg, P.; Milligan, T. Flow and sediment transport on a tidal salt marsh surface. *Estuarine, Coastal and Shelf Science* **2000**, *50*, 315–331.
9. Leonard, L.A.; Luther, M.E. Flow hydrodynamics in tidal marsh canopies. *Limnology and oceanography* **1995**, *40*, 1474–1484.
10. Nielsen, P. Turbulence effects on the settling of suspended particles. *Journal of Sedimentary Research* **1993**, *63*, 835–838.
11. Jacobs, C.N.; Merchant, W.; Jendrassak, M.; Limpasuvan, V.; Gurka, R.; Hackett, E.E. Flow scales of influence on the settling velocities of particles with varying characteristics. *PloS one* **2016**, *11*, e0159645.
12. Wang, Y.; Lam, K.M.; Lu, Y. Settling velocity of fine heavy particles in turbulent open channel flow. *Physics of Fluids* **2018**, *30*, 095106.
13. Yager, E.; Schmeeckle, M. The influence of vegetation on turbulence and bed load transport. *Journal of Geophysical Research: Earth Surface* **2013**, *118*, 1585–1601.
14. Yang, J.Q.; Nepf, H.M. Impact of vegetation on bed load transport rate and bedform characteristics. *Water Resources Research* **2019**, *55*, 6109–6124.
15. Jordanova, A.A.; James, C. Experimental study of bed load transport through emergent vegetation. *Journal of Hydraulic Engineering* **2003**, *129*, 474–478.
16. D'Alpaos, A.; Lanzoni, S.; Marani, M.; Rinaldo, A. Landscape evolution in tidal embayments: Modeling the interplay of erosion, sedimentation, and vegetation dynamics. *Journal of Geophysical Research: Earth Surface* **2007**, *112*.
17. Tinoco, R.; Coco, G. Turbulence as the main driver of resuspension in oscillatory flow through vegetation. *Journal of Geophysical Research: Earth Surface* **2018**, *123*, 891–904.
18. Wu, W.; Shields Jr, F.D.; Bennett, S.J.; Wang, S.S. A depth-averaged two-dimensional model for flow, sediment transport, and bed topography in curved channels with riparian vegetation. *Water Resources Research* **2005**, *41*.
19. Spielman, L.A. Particle capture from low-speed laminar flows. *Annual review of fluid mechanics* **1977**, *9*, 297–319.
20. Wu, L.; Gao, B.; Muñoz-Carpena, R.; Pachepsky, Y.A. Single collector attachment efficiency of colloid capture by a cylindrical collector in laminar overland flow. *Environmental science & technology* **2012**, *46*, 8878–8886.
21. Palmer, M.R.; Nepf, H.M.; Pettersson, T.J.; Ackerman, J.D. Observations of particle capture on a cylindrical collector: Implications for particle accumulation and removal in aquatic systems. *Limnology and Oceanography* **2004**, *49*, 76–85.
22. Fuchs, N.A. *The mechanics of aerosols*; Pergamon, 1964.
23. Nepf, H.M. Drag, turbulence, and diffusion in flow through emergent vegetation. *Water Resources Research* **1999**, *35*, 479–489. doi:10.1029/1998WR900069.
24. Fauria, K.E.; Kerwin, R.E.; Nover, D.; Schladow, S.G. Suspended particle capture by synthetic vegetation in a laboratory flume. *Water Resources Research* **2015**, *51*, 9112–9126. doi:10.1002/2014wr016481.
25. Wu, L.; Muñoz-Carpena, R.; Gao, B.; Yang, W.; Pachepsky, Y.A. Colloid filtration in surface dense vegetation: Experimental results and theoretical predictions. *Environmental science & technology* **2014**, *48*, 3883–3890.
26. Lamb, H. *Hydrodynamics*; University Press, 1932.

27. Langmuir, I.; Rodebush, W.; Lamer, V. Filtration of aerosols and development of filter materials. *OSRD-865, Office of Scientific Research and Development, Washington, DC* **1942**.
28. Wu, L.; Gao, B.; Muñoz-Carpena, R. Experimental Analysis of Colloid Capture by a Cylindrical Collector in Laminar Overland Flow. *Environmental Science & Technology* **2011**, *45*, 7777–7784. Publisher: American Chemical Society, doi:10.1021/es201578n.
29. Purich, A. The capture of suspended particles by aquatic vegetation. *University of Western Australia* **2006**, pp. 1–97.
30. Discflo Corporation, Santee, CA. *Discflo Disc Pumps: Installation, Operation, and Maintenance Manual*, 2003.
31. Butman, C.A. Sediment trap biases in turbulent flows: results from a laboratory flume study. *Journal of Marine Research* **1986**, *44*, 645–693.
32. Müller, M.; De Cesare, G.; Schleiss, A.J. Experiments on the effect of inflow and outflow sequences on suspended sediment exchange rates. *International journal of sediment research* **2017**, *32*, 155–170.
33. Jenzer Althaus, J.M.; Cesare, G.D.; Schleiss, A.J. Sediment evacuation from reservoirs through intakes by jet-induced flow. *Journal of Hydraulic Engineering* **2015**, *141*, 04014078.
34. Redding, T.; Devito, K. Particle densities of wetland soils in northern Alberta, Canada. *Canadian Journal of Soil Science* **2006**, *86*, 57–60.
35. Nikora, V.; Larned, S.; Nikora, N.; Debnath, K.; Cooper, G.; Reid, M. Hydraulic resistance due to aquatic vegetation in small streams: field study. *Journal of hydraulic engineering* **2008**, *134*, 1326–1332.
36. Kadlec, R.H. Overland flow in wetlands: vegetation resistance. *Journal of Hydraulic Engineering* **1990**, *116*, 691–706.
37. Nepf, H.M. Flow and transport in regions with aquatic vegetation. *Annual review of fluid mechanics* **2012**, *44*, 123–142.
38. Wright, K.; Hiatt, M.; Passalacqua, P. Hydrological connectivity in vegetated river deltas: The importance of patchiness below a threshold. *Geophysical Research Letters* **2018**, *45*, 10–416.
39. Hejduk, L.; Banasik, K. Variations in suspended sediment grain sizes in flood events of a small lowland river. *IAHS Publication* **2010**, *337*, 189–196.
40. Noe, G.B.; Harvey, J.W.; Schaffranek, R.W.; Larsen, L.G. Controls of suspended sediment concentration, nutrient content, and transport in a subtropical wetland. *Wetlands* **2010**, *30*, 39–54.
41. Aiona, A.R. Can a constructed stormwater facility remove fine particles from urban runoff? Master's thesis, University of California, Davis, 2013.
42. McKenzie, E.R.; Wong, C.M.; Green, P.G.; Kayhanian, M.; Young, T.M. Size dependent elemental composition of road-associated particles. *Science of the Total Environment* **2008**, *398*, 145–153.
43. Goring, D.G.; Nikora, V.I. Despiking acoustic Doppler velocimeter data. *Journal of hydraulic engineering* **2002**, *128*, 117–126.
44. Rouse, H. Modern conceptions of the mechanics of fluid turbulence. *Trans ASCE* **1937**, *102*, 463–505.
45. Kumbhakar, M.; Ghoshal, K.; Singh, V.P. Derivation of Rouse equation for sediment concentration using Shannon entropy. *Physica A: Statistical Mechanics and its Applications* **2017**, *465*, 494–499.
46. Stein, S.; Larsen, L.; Wingenroth, J. A functional form for particle interception in vegetated environments. *In Preparation* **2020**.
47. Schnurr, P.J.; Espie, G.S.; Allen, D.G. The effect of light direction and suspended cell concentrations on algal biofilm growth rates. *Applied microbiology and biotechnology* **2014**, *98*, 8553–8562.
48. Trulear, M.G.; Characklis, W.G. Dynamics of biofilm processes. *Journal (Water Pollution Control Federation)* **1982**, pp. 1288–1301.
49. Liu, D.; Lau, Y.; Chau, Y.; Pacepavicius, G. Simple technique for estimation of biofilm accumulation. *Bulletin of environmental contamination and toxicology* **1994**, *53*, 913–918.
50. Characklis, W.G.; Trulear, M.; Bryers, J.; Zelver, N. Dynamics of biofilm processes: methods. *Water Research* **1982**, *16*, 1207–1216.

© 2020 by the authors. Submitted to *Geosciences* for possible open access publication under the terms and conditions of the Creative Commons Attribution (CC BY) license (http://creativecommons.org/licenses/by/4.0/).